Accepted Manuscript

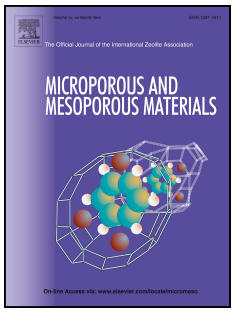

NMR cryoporometric measurements of porous silica: A method for the determination of melting point depression parameters of probe liquids

Taylor J. Rottreau, Christopher M.A. Parlett, Adam F. Lee, Rob Evans

PII: S1387-1811(18)30004-0

DOI: 10.1016/j.micromeso.2018.01.004

Reference: MICMAT 8729

To appear in: *Microporous and Mesoporous Materials*

Received Date: 2 October 2017

Revised Date: 22 November 2017

Accepted Date: 3 January 2018

Please cite this article as: T.J. Rottreau, C.M.A. Parlett, A.F. Lee, R. Evans, NMR cryoporometric measurements of porous silica: A method for the determination of melting point depression parameters of probe liquids, *Microporous and Mesoporous Materials* (2018), doi: 10.1016/j.micromeso.2018.01.004.

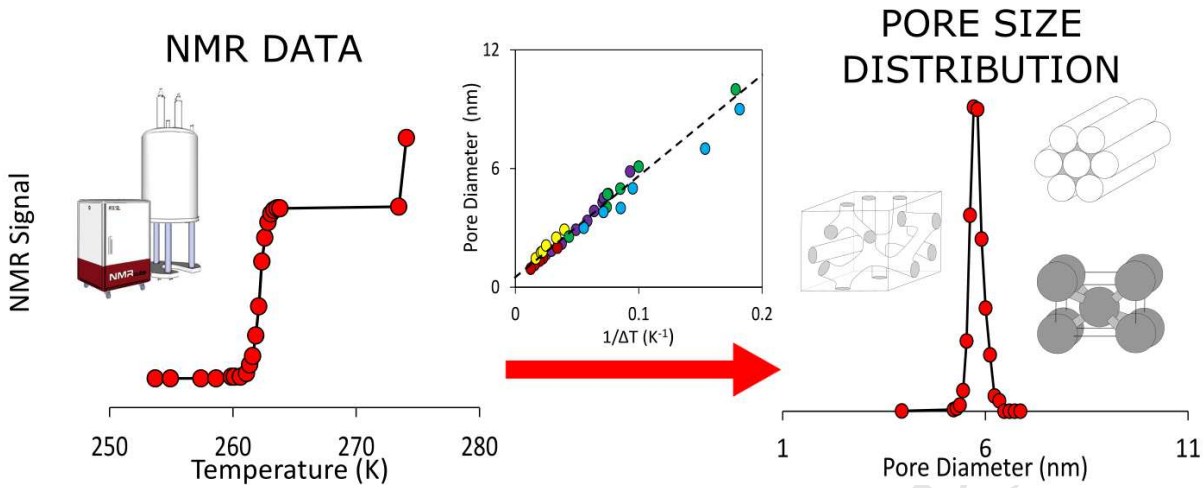

NMR Cryoporometric Measurements of Porous Silica: A Method for the Determination of Melting Point Depression Parameters of Probe Liquids.

Taylor J. Rottreau[†], *Christopher M. A. Parlett*[‡], *Adam F. Lee*[‡§] *and Rob Evans**[†]

[†]Aston Institute of Materials Research, School of Engineering and Applied Science and [‡] European Bioenergy Research Institute, Aston University, Birmingham B4 7ET, United Kingdom.

[§]Department of Chemistry, University of York, York YO10 5DD, United Kingdom.

* Corresponding author. Email address: r.evans2@aston.ac.uk

Abstract

Nuclear magnetic resonance (NMR) cryoporometry is a non-invasive method for determining the pore size distributions of materials such as porous silica. Cryoporometry has several advantages over other porometric techniques. It is able to measure the melting process in a series of discrete steps, whereas transient heat flow techniques, such as differential scanning calorimetry (DSC), have a minimum rate of measurement, and, secondly, NMR cryoporometry can analyze pore shapes with any geometry, where nitrogen porosimetry is complicated for samples with spherical pores with narrow necks. However, one key drawback of the method is that, for any one liquid observed in any one material, there is a lack of consensus in the two parameters, k_c and $2sl$, used to convert experimental NMR melting point depression data into a pore size distribution. By considering two decades worth of literature data, values for both were obtained for water in porous silica supports, in particular an estimate of a non-freezing layer between the solid ice and the inner surface of the pore. These values were used to produce pore size distributions for three silica materials, SBA-15 and KIT-6, both with cylindrical pores but possessing different structures, and SBA-16, which has spherical pores. This represents the first time KIT-6 has been characterized by the NMR method. Furthermore, this work demonstrates a general method for obtaining values for k_c and $2sl$ which can be applied to any liquid for which suitable literature data is available.

Keywords

NMR Cryoporometry
Mesoporous Silica
NMR Characterization

1. Introduction

Mesoporous silica are key to many technological applications, including catalysis [1] and drug delivery [2], due to their characteristic porous structure. Consisting of highly ordered structures, uniform pore sizes and high surface-to-volume ratios, analytical methods such as differential scanning calorimetry (DSC) [3], nitrogen porosimetry [4], neutron diffraction [5] and gas adsorption [6] can effectively probe their structures. NMR cryoporometry [7-11] has some advantages over the previously mentioned techniques as it offers a direct measurement of open pore volume and can be used for samples in the aqueous environment [7]. Its use has been demonstrated on ordered silica, such as MCM-41 [5, 12, 13] and SBA-15 [5, 14], characterizing their pore size distributions. This information is critical in the design of mesoporous silica as differences in pore sizes have significant effects on the effectiveness of these materials as catalysts [15].

Based on the Gibbs-Thomson thermodynamics for a liquid confined within a cylindrical pore [16-21], NMR cryoporometry observes a depression in the observed melting point of a confined liquid using ^{1}H NMR spectroscopy. The melting point depression for a small isolated spherical crystal of diameter x is given by

$$\Delta T_m = T_m - T_m(x) = \frac{4\gamma_{sl}T_m}{x\Delta H_f \rho_s} \quad (1)$$

where T_m is the bulk solid melting point, $T_m\,(x)$ is the melting point of a crystal with diameter x, ΔH_f is the bulk enthalpy of fusion, ρ_s is the density of the solid and γ_{sl} is the surface energy at the solid-liquid interface [22]. These values are constants for a particular liquid and can be simplified to a calibration constant denoted as k_c. The value of k_c is dependent on the liquid being used, and is also reported as dependent on pore

geometry and structure [10]. However, while the latter dependence is generally true of the melting point depression itself, k_c can be derived by several methods, which are not necessarily sensitive to pore geometry. The larger the value of k_c, the more suitable the liquid is for measuring larger pore sizes. Equation 1 relies upon a number of assumptions, such as γ_{sl} is isotropic and that the size of the crystal is large enough that it retains its bulk properties [22].

In order to convert the melting point depressions observed into a pore size distribution, a value for k_c must be known. There are several methods which have been used to calculate the value of k_c. The first method involves measuring the temperature depression for a range of different pore sizes that have been confirmed by alternative methods. A value for k_c can be estimated from experimental data [23, 24] using Equation 2.

$$\Delta T_m = \frac{k_c}{x - 2sl} \tag{2}$$

Here, x is the pore diameter, k_c is the calibration constant and sl is the contribution from a non-freezing surface layer. There are several potential problems that are associated with this approach. The main issue is the presence of a non-freezing surface layer, $2sl$. The existence of the non-freezing surface layer is expected based on the wetting theory for the wetting of the pore wall by the imbibed liquid [25]. The thickness of this layer has been debated in the literature and is based on the assumption that the layer is independent of pore size. Previous NMR studies into the behavior of water in silica systems have revealed the thickness as being between 1-3 monolayers of water, corresponding to a maximum value of approximately 0.8 nm [3, 5, 9, 10, 13, 26, 27], but with little agreement between different studies. This literature data is summarized in

Table 1 with differences in the contribution of a non-freezing surface layer resulting in the various results observed for k_c. The range of k_c values previously obtained for water lie between 49 and 58 K nm.

A value for k_c can also be estimated. Taking into account the effect of the solid/liquid interface yields the following equation, Equation 3.

$$k_C = 2\nu\gamma_{Sl}\frac{T_m}{\Delta H_f} \quad (3)$$

In this equation, ν is the molar volume of the liquid, γ_{Sl} is the surface energy at the solid-liquid interface, ΔH_f is the bulk enthalpy of fusion and T_m is the bulk melting point. When measuring the melting point depression for a liquid confined within a cylindrical pore shape, an additional factor of 2 needs to be added to Equation 2 to take into account the differences in pore curvature [10, 28, 29]. By obtaining values for molar volume, the free energy at the interface and latent heat of melting, an estimation for k_c can be obtained. Other estimations for k_c were found by using a two-parameter fit to experimental data, rather than one-parameter or linear fits. Vargas-Florencia et al. [30] describe applying this method for octamethylcyclotetrasiloxane (OMCTS) confined in large pores. OMCTS was found to have a much larger k_c value than water, making it more suitable for cryoporometry measurements of larger pores, up to a micrometer in size. However the k_c value obtained is based on assumptions of the size of γ_{Sl} [30].

Another method used to estimate k_c is to plot the freezing point depression against the surface to volume ratio [10]. The advantage of this procedure is that is does not require an assumption to be made on the pore geometry. The disadvantage however is that the surface to volume ratio needs to be determined by other techniques such as

gas adsorption [6]. A further disadvantage is that the method does not take into account the non-freezing surface layer and consequently, the value of k_c is overestimated. Despite the disadvantages, Petrov and Furo [10] describe how they have used this method to obtain values of k_c for liquids such as water and cyclohexane.

The advantages of NMR cryoporometry over other porometric techniques have been discussed in recent reviews [7, 10]. In particular, it is non-destructive, it measures the sample in a series of discrete steps, allowing for acquisition of greater signal-to-noise, and it is a direct measurement of pore volume, able to measure arbitrarily shaped pores. In this paper, an alternative method for obtaining k_c and $2sl$ is demonstrated. By fixing the value of k_c, according to the liquids' inherent properties, and studying a series of literature data from a range of experimental studies, an estimate for the thickness of the non-freezing surface layer can be determined. Different structures and geometries of the materials do not have an effect on the pore diameter measurements, as found by measuring the melting point depression of water confined in the pores of SBA-15, SBA-16 and, for the first time, KIT-6 silica.

2. Experimental

The SBA-15, SBA-16 and KIT-6 silica samples were prepared by the methods of Stucky [31] and Ryoo, [32] respectively. Successful synthesis of both supports has been confirmed by Low-angle X-Ray diffraction (XRD) and the plots for all pore sizes are provided in the supporting information. All samples were dried in the oven at 373.15 K for 24 hours and then placed in a desiccator for a further 24 hours prior to being used.

2.1.Nuclear Magnetic Resonance

Water was pipetted onto each support and the saturated silica samples were left to soak for at least 12 hours. To ensure imbibition of the liquid into the pores, the samples were transferred to a 5 mm NMR tube, sealed with parafilm and placed on the centrifuge at 1500 rpm for 1.5 hours.

All cryoporometry measurements were made using the CPMG [33, 34] pulse sequence illustrated in Figure 1. The sequence comprises a basic spin echo with a T_2 filter. With careful selection of the filter, it was possible to differentiate between the solid and liquid phases of the sample. A delay time of 4 ms ensured that the solid signal was completely removed. Care was taken to ensure excess water was present so that a rise in signal intensity for both the confined and bulk melting was observed.

In each cryoporometry experiment, a melting curve has been acquired. The sample was initially frozen, in a series of small temperature steps, beyond the freezing point of the in-pore liquid, until no NMR signal was acquired. At least 10 minutes passed after all temperature changes and NMR experiments were used to confirm no further changes in acquired signal. For each acquisition at a given temperature, 8 transients of 8192 complex data points were obtained. The typical total NMR experimental time to characterize one silica sample was 8 - 9 hrs, which compares well with about 12 hours for a full nitrogen isotherm, although these times are highly dependent on the material (degree of porosity and surface area), experimental parameters, such as rate of heating, and mass of sample analyzed.

To obtain low temperatures, a Bruker BVT3200 temperature control system, with a precision of 0.1 K, was used. The cooling system passes a combination of N_2 gas and air over the sample at a flow rate of 400 l/h operating at 4% cooling with the probe heater set to a maximum of 17% output. Before starting experimental work, the temperature control system was calibrated using a deuterated methanol NMR thermometer, producing a calibration relationship between the nominal spectrometer temperature and actual sample temperature. [35] Further calibrations were performed to determine the stability of the temperature at a given nominal spectrometer temperature and also the time taken for a given temperature change to occur. Before the start of a cryoporometry experiment, the cooling system was allowed to equilibrate with the probe heater. The temperature control unit was optimized to ensure that over- and undershoot of the sample temperature was minimized effectively. Furthermore, the probe was tuned and matched in areas out of sample phase transition to account for the significant temperature changes.

The NMR signal intensities between pore and bulk melting regions have been corrected to account for the effect of Curie's law, where the signal intensity decreases with increasing temperature outside of phase transformations [36]. The intensities are then further normalized to a value where all of the confined water is liquid and the bulk water remains frozen.

Following the approach detailed by Strange et al. [11] and using values of k_c and sl obtained in 3.1, the melting point depressions acquired by NMR cryoporometry can be converted into pore size distributions by the use of Equation 4.

$$\frac{dv}{dx} = \frac{k_c}{x^2} \cdot \frac{dv}{dT} \qquad (4)$$

Here, $\frac{dv}{dT}$ is the change in liquid volume with temperature, k_c is the calibration constant and x is the pore diameter.

2.2.Differential Scanning Calorimetry (DSC)

The DSC measurements were made using a Mettler-Toledo DSC 1 STAR^e system apparatus equipped with a liquid nitrogen cooling supply. Samples of approximately 2 mg of the dry silica were added to an aluminum pan followed by approximately 10 mg of water. The pans were then immediately sealed and re-weighed. The samples were initially taken down to 228.15 K prior to acquisition to ensure all of the liquid is frozen. A heating rate of 0.5 K min^{-1} was used through to a final temperature of 283.15 K. To transform the DSC melting curves into a pore size distribution, the procedure outlined in Majda et al. [37] was followed.

2.3.Nitrogen Porosimetry

Nitrogen porosimetry was undertaken on a Quantachrome Autosorb IQTPX porosimeter with analysis using ASiQwin v3.01 software. Samples were degassed at 523.15 K for 12 hours prior to recording N_2 adsorption/desorption isotherms. Mesopore properties were calculated applying the BJH method to the desorption isotherm for relative pressures of $P/P_0 > 0.35$.

2.4. Scanning Transition Electron Microscopy (STEM)

High resolution bright field STEM images were obtained on an aberration corrected JEOL 2100-F microscope operated at 200 kV, with image analysis using ImageJ 1.41 software. Samples were dispersed in methanol and drop cast on 200-mesh carbon coated copper grids and dried under ambient conditions.

3. Results & Discussion

3.1. Obtaining Values for k_c and $2sl$

A number of methods for estimating values of both k_c and the thickness of the non-freezing surface layer, $2sl$, have been reported in the literature for the freezing of water in silica. For example, assuming that there is no non-freezing layer, and forcing the data through the origin, a higher value of k_c is obtained. There is no consensus on the thickness of the surface layer itself, with estimated values ranging from 0 to 0.76 nm, the choice of which affects the value of k_c obtained. These values are summarized in Table 1.

We have developed an alternative method for obtaining values for the two parameters. By taking into account all of the raw melting curve data used in the references cited in Table 1, it is possible to use all measurements of the melting point of water obtained in porous silica for different pore sizes, different geometries and different structures. To the best of our knowledge, this use of all of the cryoporometric data has not been previously reported.

Figure 2 plots the pore size distributions against observed melting point depressions for 37 different materials, all with pore sizes lower than 10 nm, from 6 previous cryoporometric studies of porous silica. Characterization of the pore sizes of the silica used here was done using N_2 porosimetry. Literature values for the physical constants and parameters used in the melting point depression constant, k_c, are summarized in Table 2, were used to calculate a value of 49.53 K nm, using Equation 3, so only a single-parameter fit of the literature data, using Equation 5, is required to estimate the thickness of the non-freezing surface layer, where the line crosses the

vertical axis. The thickness of the surface layer according to Figure 5 is 0.533 ± 0.062 nm.

$$x = \frac{k_c}{\Delta T_m} + 2sl \quad (5)$$

Given the assumptions made, not only in the development of the theory (for example, enthalpy changes depend on the temperature at which they occur) but also assuming, for example, that k_c is a constant for any cryoporometry experiment using the same liquid/porous material and that $2sl$ is constant over the temperature ranges specified [13, 27, 38], the quality of the fit, with an uncertainty of 11 %, is good.

The uncertainty in pore size distributions generated from these values can be estimated from the uncertainty in $2sl$, ± 0.062 nm, and from the intrinsic error in our temperature control unit. For the experiments here, in order to characterize the pore size distributions with highest resolution, a minimum temperature ramp was employed, with an uncertainty of ± 0.04 nm estimated for a 5 nm pore size material. This gives the overall technique demonstrated here an experimental error of only ± 0.07 nm. Reduced experimental times can be achieved, with a coarser temperature ramp, but at the expense of pore size distribution resolution.

The utility of this new approach can be further illustrated by demonstrating the method with a different liquid in a different porous material; for example, cyclohexane in controlled pore glasses with pore sizes between 10 and 80 nm. Figure S9 shows a plot of reciprocal temperature depression against pore diameter for cyclohexane in glass, for 13 measurements taken from 5 references [22, 39-42], with 3 additional measurements acquired at Aston. Fitting of this data to the rearraged Gibbs-Thomson equation (Equation 4), using a value of k_c of 103.7 nm K, estimated a value for $2sl$ of 2.95 ±

0.40 nm. This compares well with previous studies [43] and corresponds to a layer of approximately 4 molecules stacked upon one another.

3.2.Pore Size Distributions of SBA-15 and KIT-6 from NMR

In order to validate the approach detailed in 3.1, pore size distributions were produced for three different types of porous silica: SBA-15, KIT-6 and SBA-16. The results of all CPMG spin echo measurements for water confined within the pores of the three porous silica materials are illustrated in Figures 3, 4 and 5. In all cases, there is an increase in signal intensity as the temperature increases and the water confined in the pores melts. A subsequent rise in signal intensity at the bulk melting temperature is also observed. Each sample demonstrates a smooth transition from solid to liquid. Those which are smaller in average diameter experience a broader pore melting transition region compared to those larger in size. A small amount of signal was observed at temperatures much less than the onset of significant melting, particularly in experiments using KIT-6. This may be due to the interconnected nature of the pores. Some water may reside in the twists of the torturous matrix and suffer a subsequent enhancement to its onset of melting. Nonetheless, this small amount of signal observed was less than 5 % in overall signal intensity when compared to the melting of the water confined within the pores.

Pore size distributions were obtained by the use of Equation 4, using the values for k_c and $2sl$, 49.53 K nm and 0.533 nm respectively, obtained from the analysis in 3.1. The pore size distributions measured for SBA-15 are shown in Figure 6. These measured pore sizes can be verified by the use of N_2 porosimetry (Figure S3) and DSC (Figure S6). To the best of our knowledge, KIT-6 has not been characterized using

NMR cryoporometry. While it has cylindrical pores, their geometry within a unit cell is different from SBA-15. Instead of packed channels, the pores form an intertwined 3-D cubic network. The pore size distributions measured for KIT-6 are shown in Figure 6. Figures S4 and S7 show the KIT-6 pore size distributions as acquired by N_2 porosimetry and DSC, respectively. The pore size distribution data for both SBA-16 and KIT-6 are summarized in Tables 3 and 4 for both silica materials, for all measurements. The NMR methods shows very good agreement with the DSC data, with a RMS error of only 5.2 %. The differences between the NMR data and N_2 porosimetry were similar at lower pore sizes, but increased to over a nanometer in the silica with larger pore sizes.

For the measurement of pore size, DSC and the NMR cryoporometry share many similarities, none more so than the fact they both measure a depression in the melting point of water confined to pores. Nitrogen porosimetry, however, measures changes in pressure as the nitrogen flows in and out of the pores. This method obtains slightly larger pore sizes than NMR and DSC for both types of silica materials studied in this work. Similar differences in estimated pore sizes have been reported elsewhere in the literature [44, 45]. In some cases, the differences have been related to the structures of the porous material. That there are differences is perhaps not surprising. For both gas adsorption and thermoporometric methods, assumptions have to be made about the phase changes being studied. In N_2 adsorption method, the molar volume and surface tension of the liquid nitrogen are required. These are normally taken as their bulk properties. In the NMR method, there are four parameters (Eqn. 3), all of which are assumed to be both constant and the same as their bulk values. A further set of assumptions made by both methods lies in the liquid-solid interface and its thickness. In this paper, we offer a method for estimation of this layer, and have used this in all of our pore size distribution estimations. For the nitrogen method, the thickness of this layer is

estimated for each pore diameter. A liquid-gas interface will also be more sensitive to changes in temperature and pressure.

STEM images were obtained for one sample of each type of silica together with the frequency percentage with respect to pore size (Figures S10 and S11). The associated pore diameters for SBA-15-3 and KIT-6-3 obtained by microscopy analysis were 5.0 nm and 5.2 nm respectively, with a maximum standard deviation of 10%. The agreement with the data provided in Tables 3 and 4 illustrate the suitability of the techniques demonstrated herein to accurately study the pore size.

3.3. Spherical Pore Size Distributions from NMR

While SBA-16 has a different, spherical, pore structure to the materials studied previously, the same pair of fitting parameters can be used to obtain pore size distributions from the melting point depression data acquired. In this case, an additional factor of 2 is required [10, 28, 29] producing the original Equation 1, obtained for an ideal spherical pore. The pore size distributions for water confined in SBA-16 are shown in Figure 8.

These pore size distributions can be verified, as before, with DSC (see S8 in the supporting information for pore size distributions acquired using DSC) and the pore size distributions are summarized in Table 5 for SBA-16 silica with four different pore sizes, between 1 and 10 nm. The NMR methods shows very good agreement with the DSC data, with a RMS error of only 1.3 %.

Verification of the pore sizes using N_2 porosimetry is hindered by the structure of the silica. If the cylindrical windows between the spherical pores are smaller than a

critical diameter (*ca*. 6 nm for nitrogen analysis), a process known as cavitation occurs, where spontaneous nucleation and growth of gas bubbles in the metastable, condensed fluid will occur. The pore size distributions calculated in these conditions no longer reflect the actual pore sizes. [46-48] Figure S5 shows pore size distributions, obtained using N_2 porosimetry, for the SBA-16 samples studied here, with the key feature of a sharp peak at a smaller pore diameter. The NMR method only measures the liquid within the pore, giving an accurate measurement of the spherical pore size.

STEM images were obtained for all SBA-16 samples to enable comparison with both thermoporometry techniques (Figure 9). The results, listed in Table 5 with a maximum standard deviation of 12%, show good correlation with both the NMR and DSC analysis. Figure S12 shows the frequency percentages with respect to pore size for each spherical sample.

Conclusions

While NMR cryoporometry is well established as an analytical method for determining pore size distributions, no real consensus has yet been reached on what values of k_c and $2sl$ to use in NMR cryoporometry experiments [10]. In the case of water, reported values of k_c range from 21 to 53 nm K while the treatment of $2sl$ ranges from it being completely neglected to values of ca. 0.8 nm reported.

This work offers values for both. Using a fixed value of k_c, based on theory, and fitting to a literature set of cryoporometric data, covering several different silica pore geometries and two decades of research, an estimate for the thickness of the non-freezing surface layer was determined for water/porous silica samples. With the values of k_c and $2sl$ obtained here, NMR cryoporometry was used to the determine pore size

distributions of porous silica with cylindrical or spherical pore structures, and different unit cell geometries. Pore size distributions have been obtained for the 2D isolated parallel pores of SBA-15, the spherical pores of SBA-16 and, for the first time, the 3D interconnected pores of KIT-6. Good agreement with pore size distributions obtained by alternative methods was achieved, validating the method for obtaining k_c and $2sl$. In particular, the pore size distributions of spherical pores were obtained; the NMR method measures the true pore diameter whereas N_2 porosimetry fails to do so here. NMR can be seen as a complementary technique here, as both measurements are critical to understanding the materials and their potential applications.

More generally, the use and analysis of literature melting point depression data demonstrated here can be applied to other liquids confined in other porous materials, with cyclohexane in glass an additional example illustrated in the SI. The methodology used to obtain these values highlights the versatility of NMR cryoporometry. No one particular liquid is suited to measuring the complete range of pore sizes and materials available. Water will not easily imbibe into hydrophobic materials and there is an upper limit to the pore sizes it can measure, determined by k_c and the temperature control of the spectrometer. Through an educated choice of probe liquid, NMR experiments can be tailored to the pore diameter and surface characteristics of the material being studied. There is a wealth of available literature data for the study of liquids in confined pores and related melting point depressions. This resource can be used to obtain suitable parameters for cryoporometric studies for many other liquids, other than water and cyclohexane.

Given that NMR spectrometers have near ubiquitous use in chemistry research, the flexibility offered by liquid choice, the capability to measure different pore

structures and geometries and the possibility of use of literature melting point data for obtaining values of k_c and $2sl$ should serve to make NMR cryoporometry more widely used, particularly in fields such as catalysis where such silica supports find wide application and the pore sizes and structures of such species has such an important role.

Acknowledgments

Financial support for a Ph.D. studentship from the School of Engineering and Applied Science, Aston University, is gratefully acknowledged. A.F.L. and C.M.A.P. were supported by the Engineering and Physical Sciences Research Council (Grant Number EP/N009924/1). We also thank Prof. Paul Topham for his contributions to improving the manuscript.

References

(1) R. Huirache-Acuna, R. Nava, C.L. Peza-Ledesma, J. Lara-Romero, G. Alonso-Nunez, B. Pawelec, E.M. Rivera-Munoz, Materials. 6 (2013) 4139-4167.
(2) R. Mellaerts, C.A. Aerts, J. Van Humbeeck, P. Augustijns, G. Van den Mooter, J.A. Martens, Chem. Commun. (2007) 1375-1377.
(3) S. Jahnert, F. Vaca Chavez, G.E. Schaumann, A. Schreiber, M. Schonhoff, G.H. Findenegg, Phys. Chem. Chem. Phys. 10 (2008) 6039-6051.
(4) R. Guillet-Nicolas, R. Ahmad, K.A. Cychosz, F. Kleitz, M. Thommes, New J. Chem. 40 (2016) 4351-4360.
(5) A. Schreiber, I. Ketelsen, G.H. Findenegg, Phys. Chem. Chem. Phys. 3 (2001) 1185-1195.
(6) E.P. Barret, L.G. Joyner, P.P. Halenda, J. Am. Chem. Soc. 73 (1951) 373-380.
(7) J. Mitchell, J.B.W. Webber, J.H. Strange, Phys. Rep. 461 (2008) 1-36.
(8) J. Strange, J. Mitchell, Characterising Porous Media. Lect. Note. Phys. Vol. 684, Springer, Berlin, 2006.
(9) K. Overloop, L. Van Gerven, J. Magn. Reson. 101 (1993) 179-187.
(10) O.V. Petrov, I. Furo, Prog. Nucl. Mag. Res. Sp. 54 (2009) 97-122.
(11) J.H. Strange, M. Rahman, E.G. Smith, Phys. Rev. Lett. 71 (1993) 3589-3591.
(12) R. Schmidt, E.W. Hansen, M. Stocker, D. Akporiaye, O.H. Ellestad, J. Am. Chem. Soc. 117 (1995) 4049-4056.
(13) O. Petrov, I. Furo, Phys. Chem. Chem. Phys. 13 (2011) 16358-16365.

(14) J.B.W. Webber, R. Anderson, J.H. Strange, B. Tohidi, J. Magn. Reson. Imaging. 25 (2007) 533-536.
(15) C. Pirez, J.M. Caderon, J.P. Dacquin, A.F. Lee, K. Wilson, ACS. Catal. 2 (2012) 1607-1614.
(16) J.W. Gibbs, The Collected Works of J. Willard Gibbs. Longmans, Green & Co, London, 1928.
(17) J.W. Gibbs, The Scientific Papers of J. Willard Gibbs, New Dover Edition. Thermodynamics. Vol. 1, Longmans, Green & Co, 1906.
(18) J. Thomson, Trans. Roy. Soc. 5 (1849) 575-580.
(19) J. Thomson, Proc. Roy. Soc. 11 (1862) 473-481.
(20) J.J. Thomson, Applications of Dynamics to Physics and Chemistry. Macmillan & Co, London, 1888.
(21) W. Thomson, Phil. Mag. Series. 42 (1871) 452-488.
(22) C.L. Jackson, G.B. Mckenna, J. Chem. Phys. 93 (1990) 9002-9011.
(23) J. Dore, B. Webber, J. Strange, H. Farman, M. Descamps, L. Carpentier, Physica. A. 333 (2004) 10-16.
(24) E.W. Hansen, R. Schmidt, M. Stöcker, J. Phys. Chem. 100 (1996) 11396-11401.
(25) J.O. Indekeu, Acta. Phys. Pol. B. 26 (1995) 1065-1100.
(26) R.T. Pearson, W. Derbyshire, J. Colloid Interf. Sci. 46 (1974) 232-248.
(27) G.H. Findenegg, S. Jahnert, D. Akcakayiran, A. Schreiber, Chem. Phys. Chem. 9 (2008) 2651-2659.
(28) C. Faivre, D. Bellet, G. Dolino, Eur. Phys. J. B. 7 (1999) 19-36.
(29) J. Riikonen, J. Salonen, V.P. Lehto, J. Therm. Anal. Calorim. 105 (2010) 811-821.
(30) D. Vargas-Florencia, O.V. Petrov, I. Furo, J. Colloid. Interf. Sci. 305 (2007) 280-285.
(31) D. Zhao, J. Feng, Q. Huo, N. Melsoh, G.H. Fredrickson, B.F. Chmelka, G.D. Stucky, Science. 279 (1998) 548-552.
(32) F. Kleitz, S.H. Choi, R. Ryoo, Chem. Commun. (2003) 2136.
(33) H.Y. Carr, E.M. Purcell, Phys. Rev. 94 (1954) 630-638.
(34) S. Meiboom, D. Gill, Rev. Sci. Instrum. 29 (1958) 688.
(35) M. Findeisen, T. Brand, S. Berger, Magn. Reson. Chem. 45 (2007) 175-178.
(36) A. Abragam, The Principles of Nuclear Magnetism. Clarendon Press, Oxford, 1961.
(37) D. Majda, W. Makowski, M. Manko, J. Therm. Anal. Calorim. 109 (2012) 663-669.
(38) J. Rault, R. Neffati, P. Judeinstein, Eur. Phys. J. B. 36 (2003) 627-637.
(39) O.V. Petrov, I. Furo, Micropor. Mesopor. Mat. 136 (2010) 83-91.
(40) L. Kimtys, D.W. Aksnes, Analyst. 132 (2007) 148-152.
(41) O.V. Petrov, I. Furo, Phys. Rev. E. 73 (2006) 011608-1-011608-7.
(42) D.W. Aksnes, L. Kimtys, Appl. Magn. Reson. 23 (2002) 51-62.
(43) S. Amanuel, H. Bauer, P. Bonventre, D. Lasher, J. Phys. Chem. C. 113 (2009) 18983-18986.
(44) Q. Zhang, Y. Dong, S. Liu, D. Elsworth, Y. Zhao, Energy. Fuels. . 31 (2017) 6951-6959.
(45) J. Riikonen, J. Salonen, M. Kemell, N. Kumar, D.Y. Murzin, M. Ritala, V.P. Lehto, J. Phys. Chem. C. 113 (2009) 20349-2034.
(46) M. Thommes, Chem. Ing. Tech. 82 (2010) 1059-1073.
(47) M. Thommes, K.A. Cychosz, Adsorption. 20 (2014) 233-250.

(48) M. Thommes, B. Smarsly, M. Groenewolt, P.I. Ravikovitch, V. Neimark, Langmuir. 22 (2006) 756-764.
(49) J.B.W. Webber, Characterising Porous Media, 2000.
(50) D. Kondrashova, R. Valiullin, Micropor. Mesopor. Mat. 178 (2013) 15-19.

Tables

Table 1. A collection of historical data summarizing values of k_c and the thickness of the non-freezing surface layer used.

k_c (K nm)	Surface layer thickness (nm)	Method used to obtain k_c	Type of porous Solid [Reference]
57.3	0	Calibration	SiO_2 [49]
49.4	0.20-0.50	Calibration	MCM-41[12]
51.4	0.60	Theoretical	MCM-41[3]
51.5	0.62	Calibration	SiO_2 [24]
52.4	0.76	Theoretical	MCM-41 + SBA-15 [5]
52	Unknown	Theoretical	SiO_2 [50]

Table 2: Literature values for the physical parameters and constants used in calculating k_c for water.

Physical Parameter	Value	Reference
molar volume of the liquid, $\boldsymbol{\nu}$ ($\mu m^3\ mol^{-1}$)	18.1	[39]
surface energy at the solid-liquid interface, $\boldsymbol{\gamma_{Sl}}$ ($mJ\ m^{-2}$)	30.0	[39]
bulk enthalpy of fusion, $\boldsymbol{\Delta H_f}$ ($kJ\ mol^{-1}$)	5.99	[39]
bulk melting point, $\boldsymbol{T_m}$ (K)	273.2	[39]

Table 3. Nitrogen porosimetry, calorimetry and NMR data for the average pore diameters of SBA-15 materials characterized in this work.

Sample	Pore Diameter – N_2 Porosimetry (nm)	Pore Diameter – DSC (nm)	Pore Diameter - NMR (nm)
SBA-15-1	3.6	3.4	3.4
SBA-15-2	3.7	3.5	3.6
SBA-15-3	5.1	4.4	4.3
SBA-15-4	6.3	5.0	4.9
SBA-15-5	7.0	5.6	5.9

Table 4. Nitrogen porosimetry, calorimetry and NMR data for the average pore diameters of KIT-6 materials characterized in this work.

Sample	Pore Diameter – N_2 Porosimetry (nm)	Pore Diameter – DSC (nm)	Pore Diameter - NMR (nm)
KIT-6-1	3.9	3.8	3.6
KIT-6-2	4.3	4.0	4.0
KIT-6-3	5.3	4.4	4.9
KIT-6-4	6.9	5.4	5.5
KIT-6-5	8.0	6.3	6.4

Table 5. Nitrogen porosimetry, calorimetry, NMR and STEM data for the average pore diameters of SBA-16 materials characterized in this work.

Sample	Pore Diameter – N_2 Porosimetry (nm)	Pore Diameter – DSC (nm)	Pore Diameter - NMR (nm)	Pore Diameter – STEM (nm)
SBA-16-1	3.1	3.6	3.5	3.7
SBA-16-2	3.3	3.9	4.0	4.2
SBA-16-3	3.5	5.6	5.5	5.3
SBA-16-4	3.6	6.3	6.5	6.5

Figures

Figure 1.

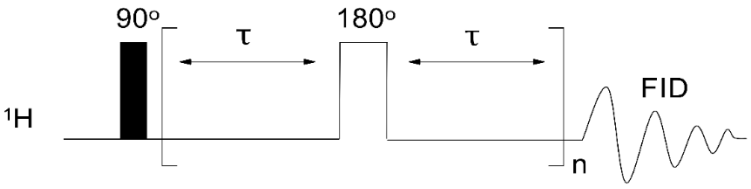

Figure 1. CPMG pulse sequence used in NMR cryoporometry experiments, with a T_2 filter of τ = 2 ms for water to ensure that the solid and liquid phases can be differentiated.

Figure 2.

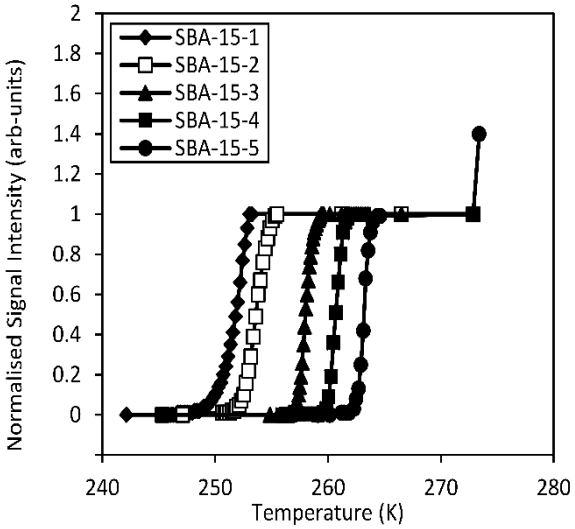

Figure 2. NMR melting curves for water confined in the pores of SBA-15 silica of different average pore diameters.

Figure 3.

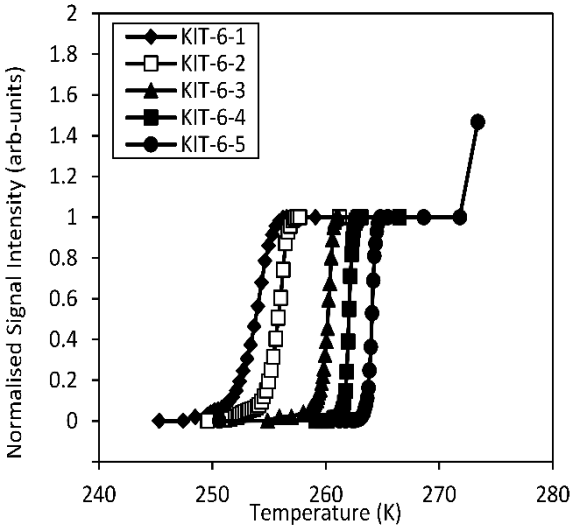

Figure 3. NMR melting curves for water confined in the pores of KIT-6 silica of different average pore diameters.

Figure 4.

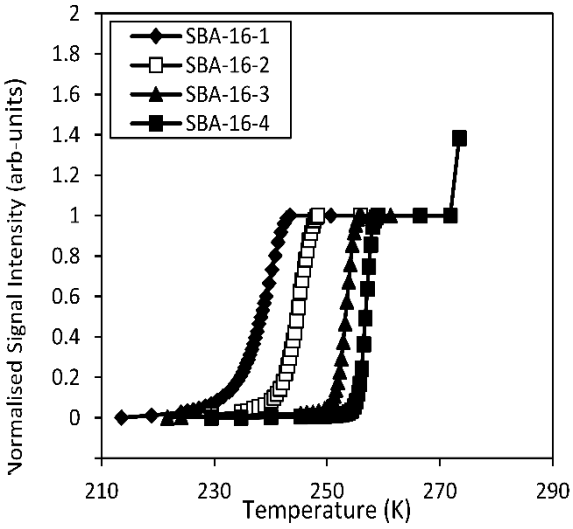

Figure 4. NMR melting curves for water confined in the pores of SBA-16 silica of different average pore diameters.

Figure 5.

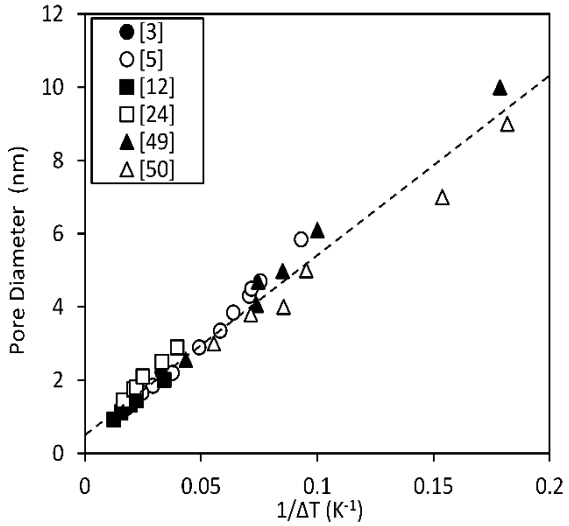

Figure 5. A plot of average pore diameter, obtained by N_2 porosimetry, *versus* the inverse of the melting point depression for the set of cryoporometry data reported in the literature. The intercept of the trend line reveals a value of 0.53 nm for the thickness of the non-freezing surface layer.

Figure 6.

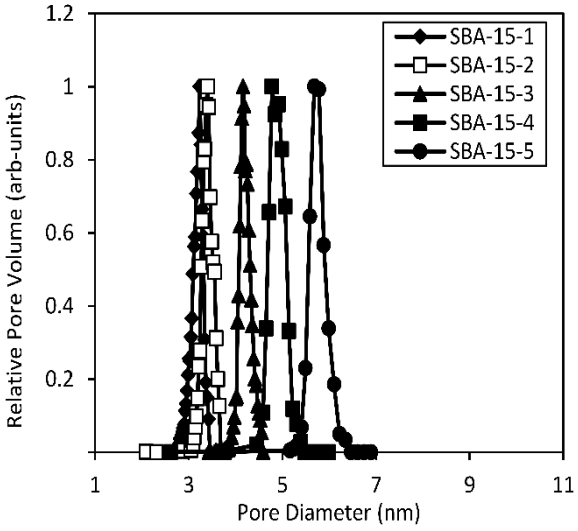

Figure 6. Pore size distributions for SBA-15 silica of five differing average pore diameters obtained by NMR cryoporometry experiments.

Figure 7.

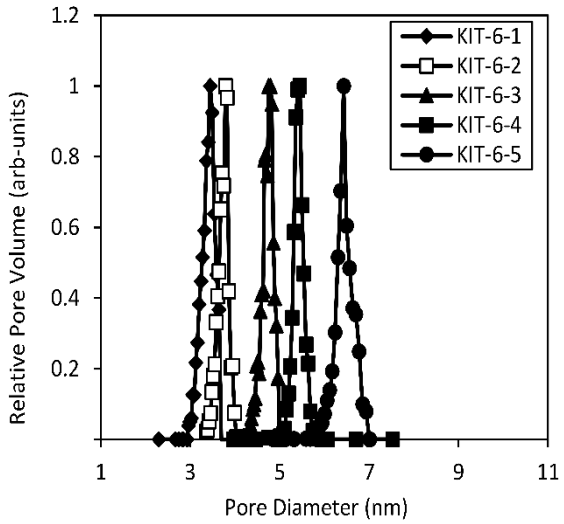

Figure 7. Pore size distributions for KIT-6 silica of five differing average pore diameters obtained by NMR cryoporometry experiments.

Figure 8.

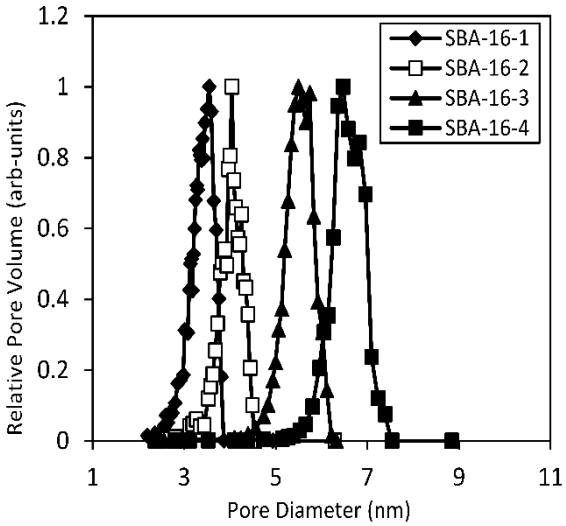

Figure 8. Pore size distributions for SBA-16 silica of four differing average pore diameters obtained by NMR cryoporometry experiments.

Figure 9.

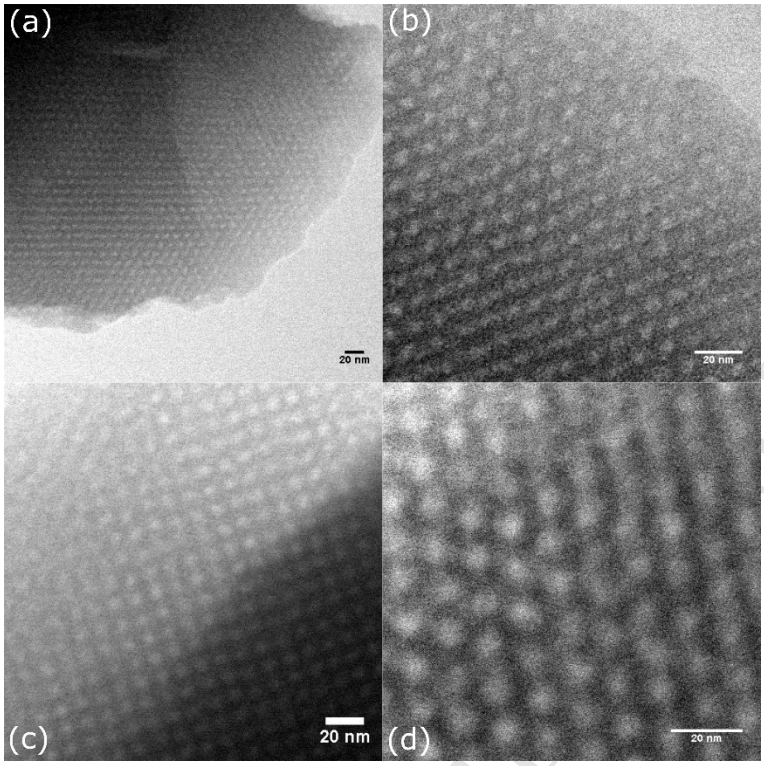

Figure 9. Bright field STEM images of the spherical pores in a) SBA-16-1 (3.7 nm), b) SBA-16-2 (4.2 nm), c) SBA-16-3 (5.3 nm) and d) SBA-16-4 (6.5 nm).

Figure captions

Figure 1. CPMG pulse sequence used in NMR cryoporometry experiments, with a T_2 filter of τ = 2 ms for water to ensure that the solid and liquid phases can be differentiated.

Figure 2. NMR melting curves for water confined in the pores of SBA-15 silica of different average pore diameters.

Figure 3. NMR melting curves for water confined in the pores of KIT-6 silica of different average pore diameters.

Figure 4. NMR melting curves for water confined in the pores of SBA-16 silica of different average pore diameters.

Figure 5. A plot of average pore diameter, obtained by N_2 porosimetry, *versus* the inverse of the melting point depression for the set of cryoporometry data reported in the literature. The intercept of the trend line reveals a value of 0.53 nm for the thickness of the non-freezing surface layer.

Figure 6. Pore size distributions for SBA-15 silica of five differing average pore diameters obtained by NMR cryoporometry experiments.

Figure 7. Pore size distributions for KIT-6 silica of five differing average pore diameters obtained by NMR cryoporometry experiments.

Figure 8. Pore size distributions for SBA-16 silica of four differing average pore diameters obtained by NMR cryoporometry experiments.

Figure 9. Bright field STEM images of the spherical pores in a) SBA-16-1 (3.7 nm), b) SBA-16-2 (4.2 nm), c) SBA-16-3 (5.3 nm) and d) SBA-16-4 (6.5 nm).

Highlights

- NMR cryoporometry used to determine pore size distributions in SBA-15, SBA-16 and, for the first time, KIT-6 silica.
- Reliable estimate of key parameters, such as the non-freezing surface layer between water and silica, obtained.
- Demonstration of a robust use of an NMR method to measure silica, independent of pore structure, for pores < 10 nm.